Supplement of Atmos. Chem. Phys., 16, 6421–6439, 2016
http://www.atmos-chem-phys.net/16/6421/2016/
doi:10.5194/acp-16-6421-2016-supplement

Atmospheric Chemistry and Physics Open Access EGU

Supplement of

Optical properties of atmospheric fine particles near Beijing during the HOPE-J^{3}A campaign

Xuezhe Xu et al.

Correspondence to: Weixiong Zhao (wxzhao@aiofm.ac.cn) and Weijun Zhang (wjzhang@aiofm.ac.cn)

S1 System performance

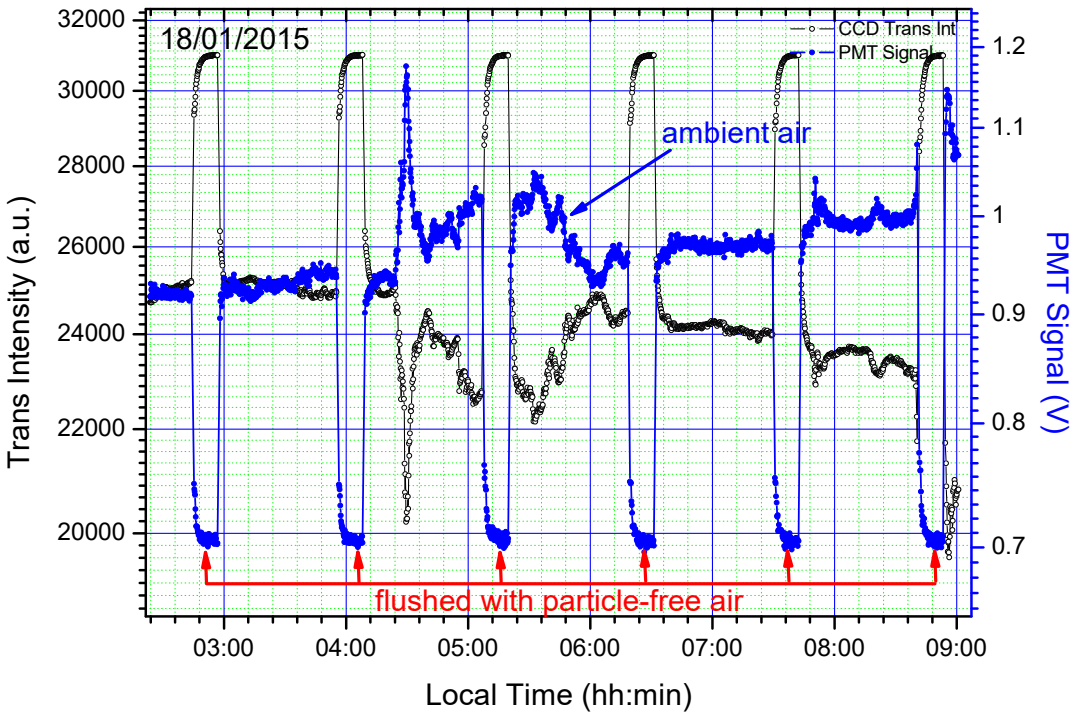

Fig. S1 Example data of the transmitted intensity measured with the CCD spectrometer and the scattering signal measured with the PMT of the cavity-enhanced abldoemeter during the experimental period. The cavity was flushed with particle-free air every hour to acquire the $I_0(\lambda)$ spectrum. No obvious drift in the LED light intensity was observed even after 6 hours of measurement, indicating the high stability of the instrument under these operating conditions.

S2 Chemical apportionment of aerosol optical properties

Chemical apportionment of light extinction of $PM_{1.0}$ was determined with a revised IMPROVE (Interagency Monitoring of Protected Visual Environments) algorithm (Pitchford et al., 2007). Although the IMPROVE algorithm is a simplified predictor of extinction, it is nevertheless a useful tool to estimate the contribution of different particle components to haze levels (Pitchford et al., 2007). Light extinction at λ = 550 nm can be estimated by multiplying the mass concentrations by component-specific mass extinction efficiencies (MEEs) of each of seven major components: sulfate (assumed to be ammonium sulfate), nitrate (assumed to be ammonium nitrate), organic mass (OM, based on the measured mass concentration of organic carbon, OC), elemental carbon (EC), fine soil, sea salt (chlorine, Cl), and coarse mass (the differences between PM_{10} and $PM_{2.5}$ mass concentration). It can be expressed by the following (Pitchford et al., 2007):

$$\begin{aligned}\alpha_{ext,550nm} \approx\ & 2.2\times f_s(\mathrm{RH})\times[\text{Small Sulfate}]+4.8\times f_L(\mathrm{RH})\times[\text{Large Sulfate}]\\ &+2.4\times f_s(\mathrm{RH})\times[\text{Small Nitrate}]+5.1\times f_L(\mathrm{RH})\times[\text{Large Nitrate}]\\ &+2.8\times[\text{Small Organic Mass}]+6.1\times[\text{Large Organic Mass}]\\ &+10\times[\text{Elemental Carbon}]+1\times[\text{Fine Soil}]\\ &+1.7\times f_{ss}(\mathrm{RH})\times[\text{Sea Salt}]+0.6\times[\text{Coarse Mass}]\\ &+\text{Rayleigh scattering (site specific)}+0.33\times[NO_2(\text{ppb})]\end{aligned} \quad \text{(S1)}$$

where f(RH) is the water growth factor of inorganic components, $f_S(RH)$ and $f_L(RH)$ are the water growth factors for the small and large particle size modes for sulfate and nitrate, respectively, and $f_{SS}(RH)$ is the hygroscopic growth factor for sea salt.

The large and small parts are defined by the IMPROVE formula as (Pitchford et al., 2007; Cao et al., 2012):

$$[\text{Large X}] = [\text{Total X}]^2/20, \text{ for } [\text{Total X}] < 20\ \mu g\ m^{-3}$$

$$[\text{Large X}] = [\text{Total X}], \text{ for } [\text{Total X}] \geqslant 20\ \mu g\ m^{-3}$$

$$[\text{Small X}] = [\text{Total X}] - [\text{Large X}]$$

where X = sulfate, nitrate or OM. The concentration of ammonium sulfate ($[(NH_4)_2SO_4]$) was 1.375 times the sulfate concentration ($[SO_4^{2-}]$), and the ammonium nitrate ($[NH_4NO_3]$) was 1.29 times the nitrate concentrations ($[NO_3^-]$). The OM concentration was estimated by multiplying the reported OC concentration by a factor of 1.6 (Turpin and Lim, 2001). The sea salt mass concentration was estimated by multiplying the Cl^- mass concentration by a factor of 1.8. The ammonium cation was

not used directly in the IMPROVE algorithm. It was assumed to be fully neutralized by SO_4^{2-} and NO_3^- and treated as ammonium sulfate ($(NH_4)_2SO_4$) and ammonium nitrate(NH_4NO_3), respectively.

The revised IMPROVE algorithm above was parameterized for atmospheric aerosol extinction at λ = 550 nm. In this study, the optical properties of $PM_{1.0}$ were measured at λ = 470 nm. The IMPROVE algorithm needs to be refined to better represent the chemical apportionment of light extinction for $PM_{1.0}$ particles. Since dry $PM_{1.0}$ aerosols were measured, the coarse mass and the hygroscopic increase of inorganic component were ignored for the inputs of the IMPROVE algorithm. The fine soil component was also left out in apportioning the extinction coefficient due to its small fraction of $PM_{1.0}$ particles during wintertime in Beijing (Sun et al., 2014).

Under the assumptions of the IMPROVE algorithm (in which particles are treated as separate entities), the difference in the wavelength will only affect the dry mass extinction efficiency terms. We modified the MEE terms in equation (S1) of each individual particle components with a scaling factor so as to be directly comparable to measurements at λ = 470 nm. The scaling factor was the ratio of the MEEs of each species at λ = 470 nm and λ = 550 nm calculated with Mie theory from the literature reported complex refractive index (Table S1) and the measured mean number size distribution.

Table S1 Densities and complex refractive indexes of different types of aerosols. (adapted from Cheng et al., 2008)

Chemical Species	Density (g cm^{-3})	Complex Refractive Index
$(NH_4)_2SO_4$	1.748	1.54 - 10^{-7} i
NH_4NO_3	1.725	1.54 - 10^{-7} i
OM	1.4	1.55 - 0.001 i
Sea salt	2.0	1.54 - 10^{-7} i
EC	1.5	1.80 - 0.54 i

Under the assumption that particles were completely separated (externally mixed) and can be adequately estimated as separate terms of each single chemical component, *j*, the extinction coefficient of component *j* can be calculated from (Bohren and Huffman, 1998; Petersson et al., 2004; Hand and Malm, 2007):

$$\alpha_{ext,j} = \int_0^\infty \frac{\pi}{4} D_p^2 Q_{ext}(m_j, D_p, \lambda) N(D_p) dD_p \qquad \text{(S2)}$$

where $N(D_p)$ is the number of particles with mean diameter D_p per unit volume in the size bin dD_p, and $m = n + ik$ is the complex refractive index. Q_{ext} is the extinction efficiency and can be calculated with Mie theory for spherical particles.

The mass extinction efficiency(MEE) is a function of the Mie extinction efficiency, particle diameter and species density (ρ_j) (Hand and Malm, 2007):

$$MEE_j = \frac{3}{2}\frac{Q_{ext}(m_j, D_p, \lambda)}{\rho_j D_p} \quad \text{(S3)}$$

If the mass size distribution of each species j does not vary with total mass concentration, the light extinction coefficient of species j can be calculated with :

$$\alpha_{ext,j} = MEE_j M_j \quad \text{(S4)}$$

where M_j is the mass concentration per unit volume.

If the mass size distribution of each species varies with the total mass concentration, the following equation can be used for the MEE calculation (Cheng et al., 2008; Cheng et al., 2015).

$$MEE_j = \frac{\sum_{bin=1}^{D_{bin}} MEE(j, D_{bin}) M_{j,bin}}{\sum_{bin=1}^{D_{bin}} M_{j,bin}} \quad \text{(S5)}$$

The total extinction is a linear combination of all the species :

$$\alpha_{ext} = \sum_j MEE_j M_j \quad \text{(S6)}$$

Since the size-segregated mass concentration of each chemical composition was not available in this work. Equation S5 was not used. We used equation (S3) (with literature reported complex refractive index, table S1, and the measured mean size distribution) for the calculation of the MEE values at λ = 470 nm and λ = 550 nm.

Under the assumptions of the IMPROVE algorithm (in which particles are treated as separate entities), the difference in the wavelength will only affect the dry mass extinction efficiency (MEE) terms. We modified the MEE terms (equation S1) of each individual particle components with a scaling factor so as to be directly comparable to measurements at λ = 470 nm. The scaling factor ($Scaling\ factor_j = MEE_{j,\lambda=470nm} / MEE_{j,\lambda=550nm}$) was the ratio of the MEEs of each species at λ = 470 nm and λ = 550 nm, calculated with equation (S3) under different pollution days was shown in Fig.

S2. As an average result, the calculated dry mass extinction efficiencies of inorganic mass (including sulfate, nitrate and sea salt), organic mass and element carbon at λ = 470 nm were 1.31, 1.30 and 1.08 times larger than that at λ = 550 nm.

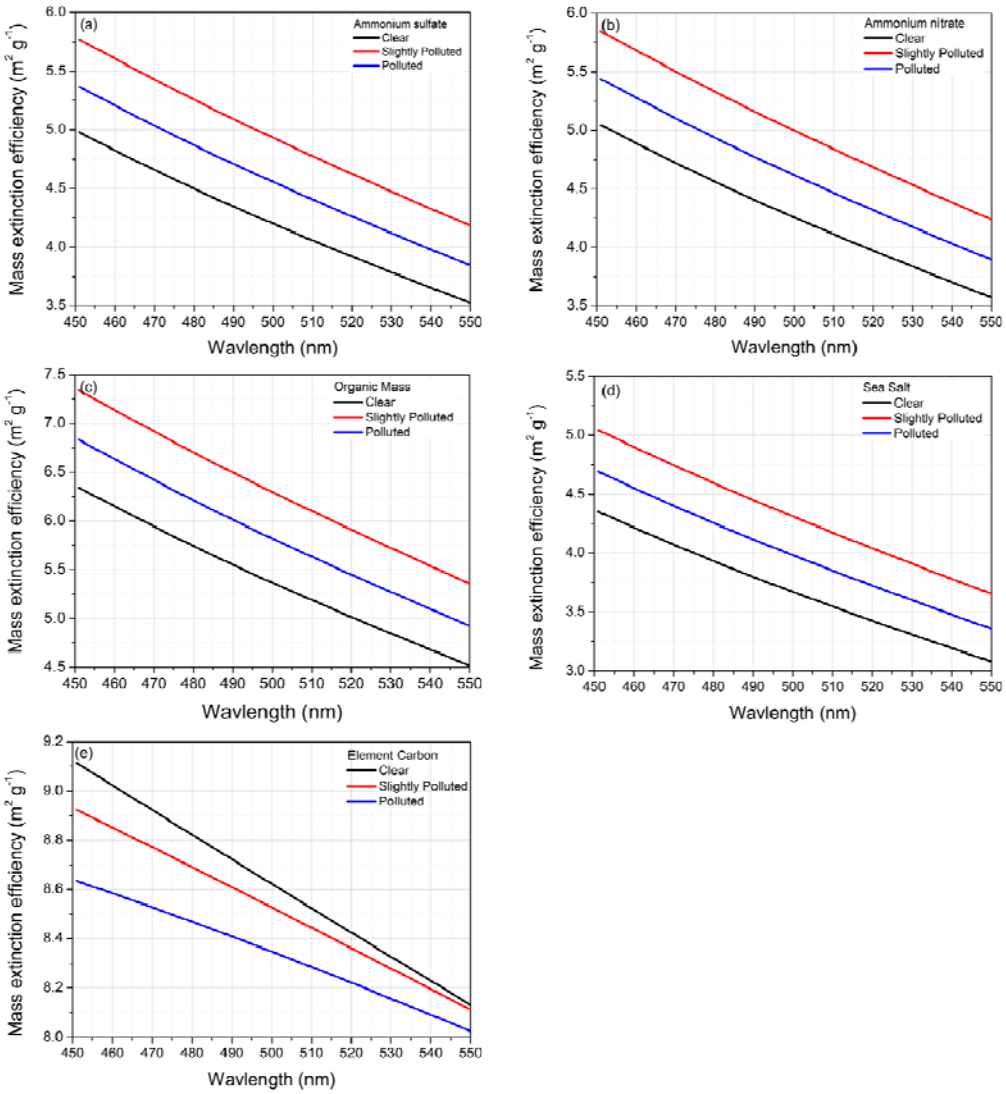

Fig. S2 Calculated wavelength dependent mass extinction efficiencies of inorganic mass (including sulfate, nitrate and sea salt), organic mass and element carbon.

The dry mass extinction efficiencies of inorganic mass (including sulfate, nitrate and sea salt), organic mass, and elemental carbon for the input of the IMPROVE formula at λ = 470 nm should accordingly be scaled by factors of 1.31, 1.30 and 1.08, respectively. The modified IMPROVE function for PM1.0 extinction at λ = 470 nm can be rewritten as following:

$$\begin{aligned}\alpha_{ext,470nm,PM_{1.0}} \approx\ & 2.88\times[\text{Small Sulfate}]+6.29\times[\text{Large Sulfate}]\\ & +3.14\times[\text{Small Nitrate}]+6.68\times[\text{Large Nitrate}]\\ & +3.64\times[\text{Small Organic Mass}]+7.93\times[\text{Large Organic Mass}]\\ & +10.8\times[\text{Elemental Carbon}]+2.23\times[\text{Sea Salt}]\end{aligned} \quad \text{(S7)}$$

The $PM_{1.0}$ mass concentration can be reconstructed as the sum of its major chemical components (Pitchford et al., 2007):

$$\begin{aligned}\text{Reconstructed mass\_}PM_{1.0} &= [(NH_4)_2SO_4] + [NH_4NO_3] + [SS] + [OM] + [EC]\\ &= 1.375\times[SO_4^{2-}] + 1.29\times[NO_3^-] + 1.8\times[Cl^-] + 1.6\times[OC] + [EC]\end{aligned} \quad \text{(S8)}$$

Studies in other Chinese megacities, such as Shanghai (Cheng et al., 2015) and Guangzhou (Tao et al., 2014), and data from US monitoring sites show that the revised IMPROVE algorithm underestimates the $PM_{2.5}$ extinction under high aerosol loading but overestimates the values under low aerosol loading. The underestimation and overestimation ratios in different studies ranged from -11 to -26 % and +25 to +54 %, respectively (Cheng et al., 2015). In this work, $\alpha_{ep,470}$ of $PM_{1.0}$ particles was reconstructed using the modified IMPROVE algorithm based on the measured concentrations of each composition (Fig. S3a), which correlated well with the measured $\alpha_{ep,470}$ (R^2 = 0.96) during this campaign (Fig. S3c). With modified IMPROVE function (Eq. S7), the agreement between the measured and calculated $PM_{1.0}$ extinctions is good (with a slope of 1.04 ± 0.04) when the measured extinction coefficient is lower than 300 Mm^{-1} (as shown in the insert of Fig. S3c). When the observed extinction coefficients are larger than 300 Mm^{-1}, the reconstructed values of the modified IMPROVE algorithm were 16% lower than observed values (calculated from the average of the ratios of the measured extinction to the reconstructed extinction for all points > 300 Mm^{-1}). The modified IMPROVE algorithm for $PM_{1.0}$ at λ = 470 nm represents the chemical apportionment of light extinction quite well. The reconstructed $PM_{1.0}$ mass concentration (Fig. S3b) using the modified IMPROVE algorithm was well correlated with the measured $PM_{1.0}$ mass concentration (the summation of the concentrations of eight water-soluble ion compositions and carbon concentration (including elemental carbon, [EC], and organic mass, 1.6×[OC])) (R^2 = 0.99, slope = 1.00, intercept = 0.28) (Fig. S3d), indicating that the modified IMPROVE algorithm can be used to estimate the chemical apportionment for extinction in this campaign.

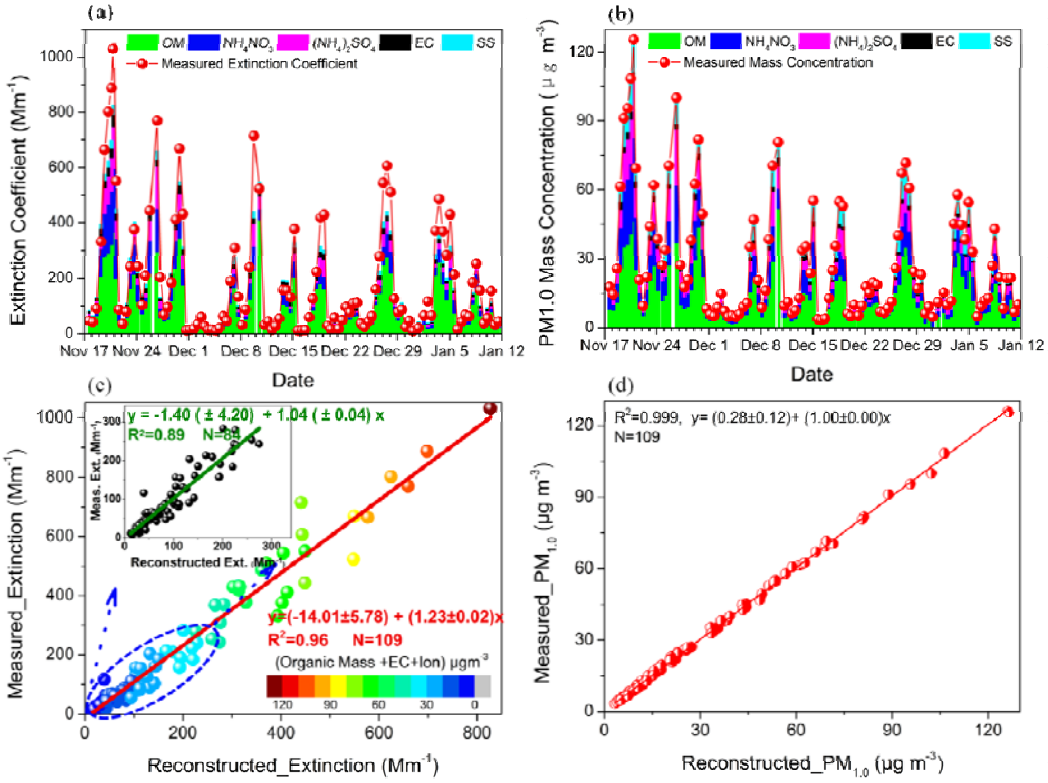

Fig. S3 (a) and (b) : The plot of measured and reconstruction value of the extinction and mass concentration, respectively; (c) and (d) : Scatter plot of the measured extinction coefficient at $\lambda = 470$ nm and $PM_{1.0}$ mass concentration against the reconstructed values with the modified IMPROVE formula. Insert of (c) shows the linear regression between measured and reconstructed extinction coefficient under lower aerosol load condition (with extinction smaller than 300 Mm^{-1}).

S3 Relationships between aerosol optical properties and wind direction

The local wind direction and wind speed were measured on the roof of building with a Gill MetPak-Ⅱ weather station. Fig. S4 presents the relationship of $\alpha_{sp,470}$, $\alpha_{ap,470}$ and ω_{470} to local wind directions and wind speed during the campaign. On these graphs, Beijing centre would be at ~206°. Fig. S4a and S4b display the wind direction versus wind speed, with $\alpha_{sp,470}$ and $\alpha_{ap,470}$ as the color scale. From November 2014 to January 2015, the winds were mostly from the southeast and southwest. There was no obvious correlation between extensive optical properties and wind direction. The average wind speed was 1.2 m s^{-1} during the field campaign. When the instantaneous wind speeds were higher than the average wind speed, the values of $\alpha_{sp,470}$ and $\alpha_{ap,470}$ decreased. The average values of $\alpha_{sp,470}$ for $v < 1.2$ m s^{-1} and $v > 1.2$ m s^{-1} were 198 Mm^{-1} and 54 Mm^{-1}, respectively. Similarly, the average values of $\alpha_{ap,470}$ for $v < 1.2$ m s^{-1} and $v > 1.2$ m s^{-1} were 41 Mm^{-1} and 11 Mm^{-1}, respectively. When $v > 1.2$ m s^{-1}, lower values of $\alpha_{sp,470}$ (< 100Mm^{-1}) and $\alpha_{ap,470}$ (< 50Mm^{-1}) occurred more frequently when the local wind came from 225 - 270°, which indicated that the air parcel was relatively clean in the wind direction. When $v < 1.2$ m s^{-1}, values of $\alpha_{sp,470}$ and $\alpha_{ap,470}$ occurred similar frequently and ranged widely when the local wind same from the south. Fig. S4c shows the relationship between the wind direction and ω_{470}, with the color scale as wind speed. The average value of ω_{470} ranged from 0.7 to 0.9 and was not strongly correlated with the wind direction. However, higher values ω_{470} (0.9 - 1.0) occurred more frequently when the local wind came from 270 - 160°, which indicated that the air parcel in this wind direction contained less light absorbing particulate matter.

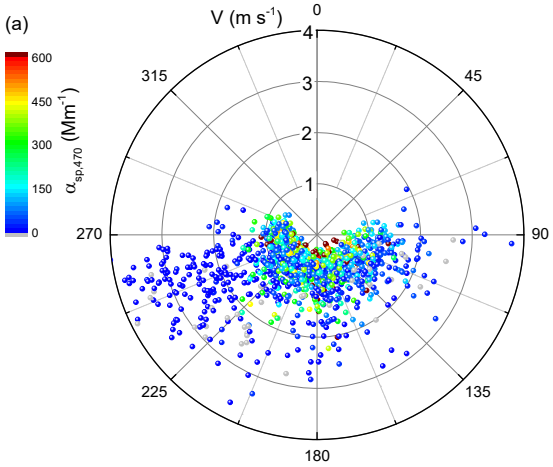

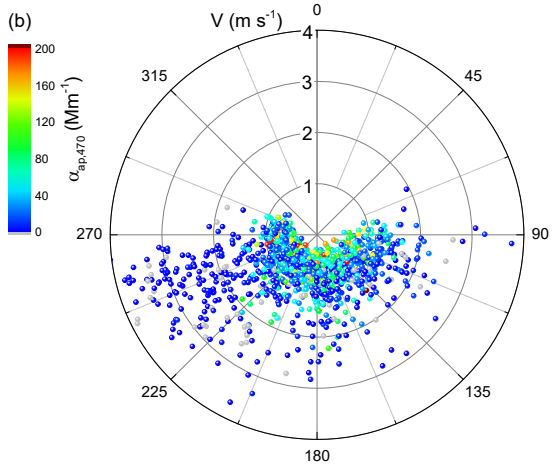

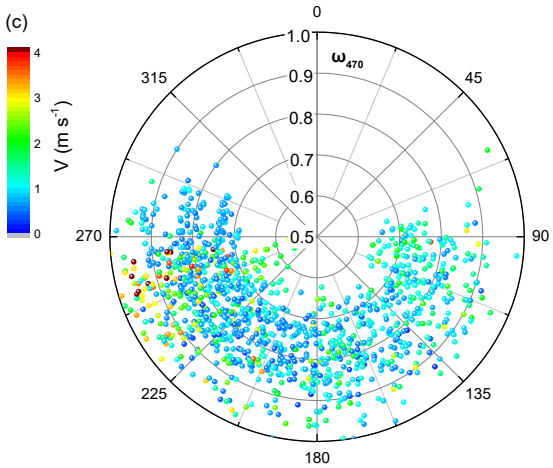

Fig. S4 Local wind direction and wind speed plots for the campaign: (a) wind direction versus wind speed (m s^{-1}), with $\alpha_{sp,470}$ (Mm^{-1}) as the color scale, (b) wind direction versus wind speed (m s^{-1}), with $\alpha_{ap,470}$, (Mm^{-1}) as the color scale, and (c) wind direction versus ω_{470}, with the color scale as wind speed (m s^{-1}).

S4 Frequency distribution and diurnal variations of dry PM1.0 optical properties

With increasing pollutant level, the extensive optical properties ($\alpha_{ep,470}$, $\alpha_{sp,470}$ and $\alpha_{ap,470}$) increased strongly, in accordance with the expected, strong dependence of particle size on light scattering. In contrast, changes in the intensive optical properties (ω_{470}) were more modest. The optical measurement data are presented as histograms of the relative frequency of occurrence of $\alpha_{ep,470}$, $\alpha_{sp,470}$, $\alpha_{ap,470}$ and ω_{470} (Fig. S5). Approximately 71% of extinction and scattering coefficients values were lower than 200 Mm^{-1} and nearly 80% of absorption coefficient values were located in the range of 1.5–50 Mm^{-1}. Approximately 90% of the ω_{470} values fell into the range of 0.70–0.97. Compared with polluted days, the frequency distribution of the SSA showed similar patterns, and the average values were similar on clear and slightly polluted days.

The diurnal variations of hourly averaged extinction, scattering, absorption coefficient and SSA on clear, slightly polluted and polluted days are presented in Fig. S6. Broadly similar patterns were observed for the extensive optical properties for different pollutant levels, although diurnal variability was weak under polluted conditions owing to the high number of pre-existing particles and to the weakened diurnal changes in the boundary layer height that typically prevails under these conditions (Yang et al., 2015; Gao et al., 2016). Extinction ($\alpha_{ep,470}$) and scattering ($\alpha_{sp,470}$) tended to be lower during daytime and higher at night, in accordance with a lower nocturnal boundary layer height (Ma et al., 2011). Emissions associated with morning rush hour are apparent in the aerosol optical properties, especially in clean and slightly polluted conditions. $\alpha_{ep,470}$ and $\alpha_{sp,470}$ increased slowly in the morning (07:00–09:00 LT) to peak values at 09:00 LT, indicating significant emission and formation of particles during this period; these properties then decreased slowly until about 14:00 LT. The maximum values of $\alpha_{ap,470}$ and lowest SSA values occurred during the traffic rush hour and are therefore attributed to direct emissions of light absorbing species from vehicles. We note that the increase in $\alpha_{ap,470}$ from 06:00 to the maximum at 08:00 to 09:00 LT varied from 10 to 20 Mm^{-1} and was quite consistent across different pollutant days. This observation suggests that the number and type of particles emitted during this time period is not strongly influenced by pre-existing pollutant levels, but mainly determined by relatively constant daily emissions from traffic.

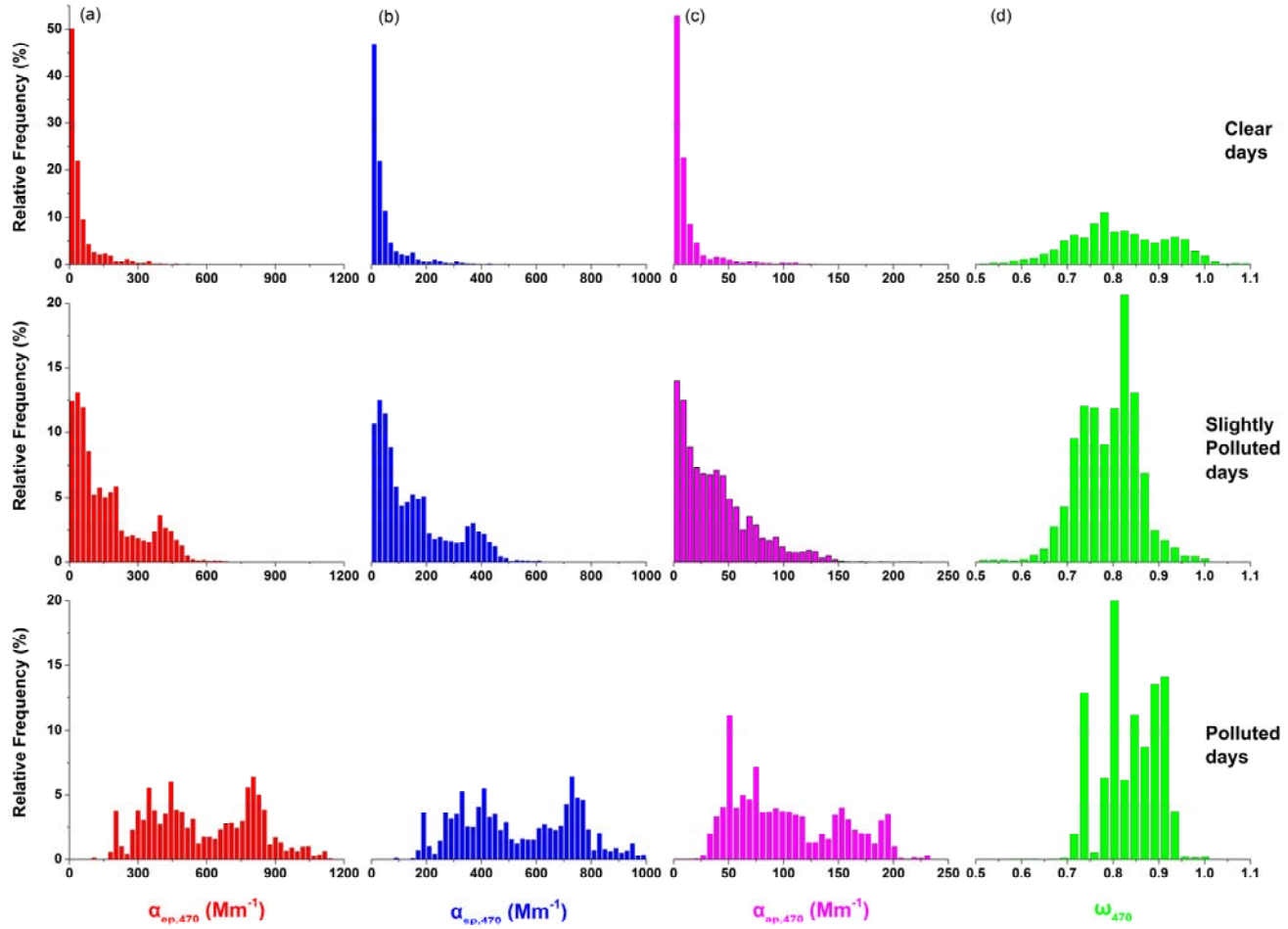

Fig S5 The frequency distributions of dry $PM_{1.0}$ optical properties at λ = 470 nm observed during the campaign. (a) extinction coefficient, (b) scattering coefficient, (c) absorption coefficient, (d) single scattering albedo on clear, slightly polluted and polluted days.

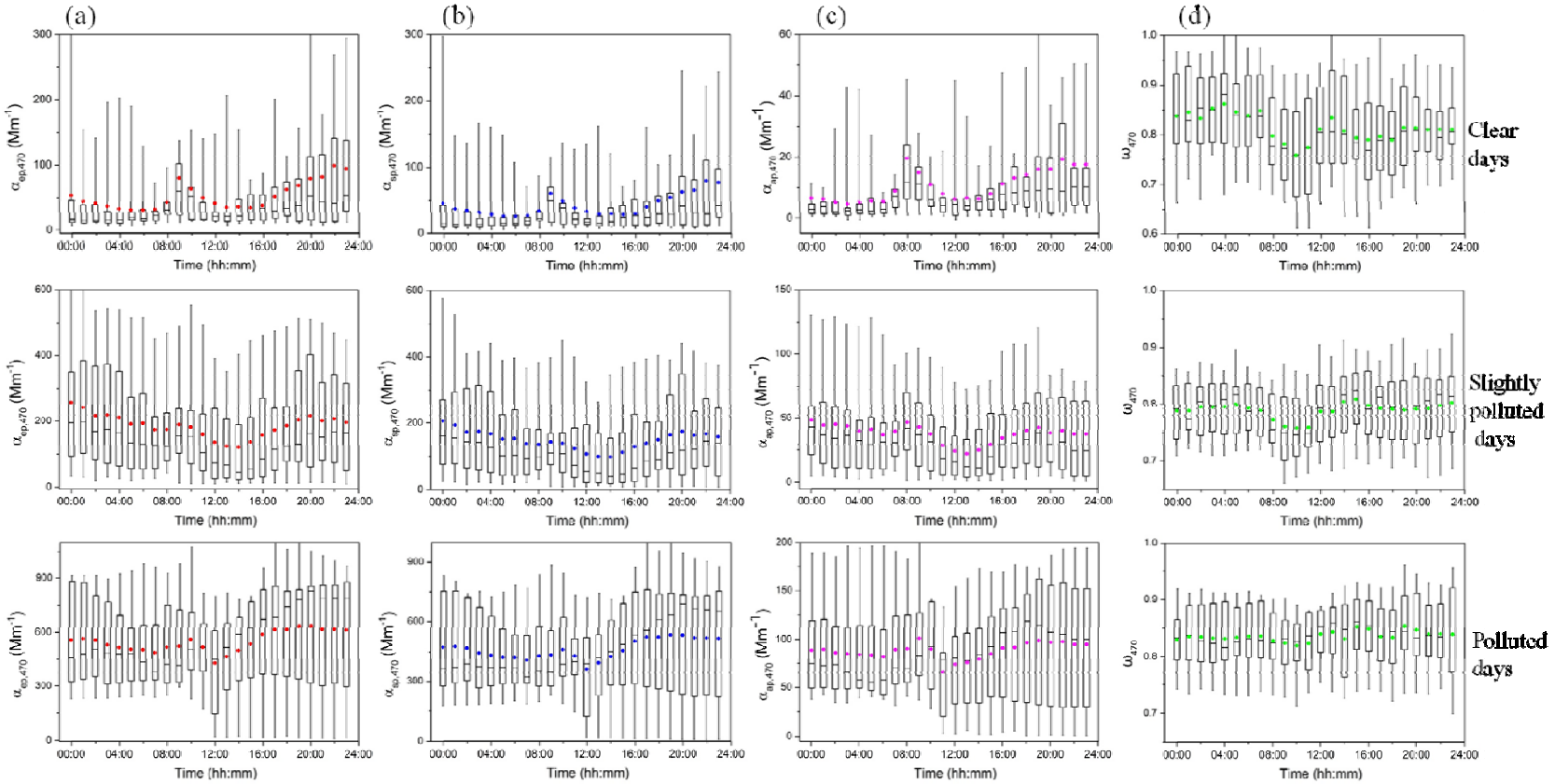

Fig. S6 Diurnal variations of hourly averaged (a) extinction coefficient, (b) scattering coefficient, (c) absorption coefficient and (d) SSA at λ = 470 nm on clear, slightly polluted and polluted days. The error bars are 5th and 95th percentiles and the limits of the boxes represent 25th and 75th percentiles.

S5 Comparison of the measured aerosol optical properties to those at other locations

The Huairou site is a new suburban site at which aerosol optical properties have not previously been reported. To put our observations at Huairou in context, the scattering and absorption coefficients and SSA observed in this campaign are compared in Table S2 to those at other locations (urban, suburban, and rural sites). As would be expected given the high concentrations of particulate matter in much of China, the mean $\alpha_{sp,470}$ value at Huairou was considerably higher than values observed in America and Europe, including the Los Angeles basin measurements in Pasadena (Thompson et al., 2012) and the urban site of Granada (Titos et al., 2012). Within China, the Huairou values for scattering and absorption were higher than in Shanghai (Li et al., 2013) and similar to the urban site of Guangzhou in China (Garland et al., 2008). Compared with other non-urban polluted sites in China, both $\alpha_{sp,470}$ and $\alpha_{ap,470}$ at Huairou were lower than Xinken (Cheng et al., 2008), Yufa (Garland et al., 2009) and much lower than Xianghe (Li et al.,2007). Moreover, the $\alpha_{sp,470}$ values were comparable to those observed at Shangdianzi, an atmospheric background site located ~150 km northeast of the urban center of Beijing (Yan et al., 2008). The average value of $\alpha_{ap,470}$ at Huairou was lower than those seen at other urban and suburban locations in China, with the exceptions of Guangzhou (reflecting the lower SSA values observed in Huairou) and the rural site of Shangdianzi.

The regional differences in SSA can be considered in terms of the different sources of particles, including local primary emissions, transport emissions and secondary aerosol formations. The average value of ω_{470} at Huairou was 0.80 ± 0.08, which was lower than suburban sites in Xinken (0.83 ± 0.05), Xianghe (0.81–0.85) and Yufa (0.86 ± 0.07), and rural sites in Shangdianzi (0.88 ± 0.05), and Pasadena (0.92 ± 0.08). Compared to urban sites, the Huairou SSA was similar to observations in Beijing (0.80 ± 0.09) (He et al., 2009), but considerably higher than in Shanghai (0.70 ± 0.07) (Li et al., 2013) and Granada (0.71 ± 0.07) (Titos et al., 2012). The lower SSA values probably arose from the higher contribution of vehicular emissions in Shanghai (Zhou et al., 2009) and both traffic emissions and a higher mass fraction of light absorbing particles caused by fuel-oil combustion in Granada (Titos et al., 2012).

Table S2. List of the mean values of aerosol scattering, absorption coefficients, and single scattering albedo in this campaign and recently reported values from references.

Location	Date (MM/yy)	λ (nm)	α_{sp} (Mm^{-1})	α_{ap} (Mm^{-1})	ω_0	RH	Inlet	References
Granada, Spain (Urban)	03/2006 - 02/2007	α_{sp} : 550	61±25	24±9	0.71±0.07	＜50%	PM_{10}	Titos et al.(2012)
		α_{ap} : 550						
Guangzhou (Urban)	07/2006	α_{sp} : 550	151±103	34±27	0.82±0.07	＜40%	PM_{10}	Garland et al.(2008)
		α_{ap} : 532						
Beijing (Urban)	01/2005 - 12/2006	α_{sp} : 525	255±243	45±39	0.80±0.09	＜60%	TSP	He et al.(2009)
		α_{ap} : 532						
Shanghai (Urban)	04 - 05/2010	α_{sp} : 532#	102±74	44±35	0.70±0.07	41.2%	TSP	Li et al.(2013)
		α_{ap} : 532						
Xinken, PRD (Suburban)	10/2004 - 11/2004	α_{sp} : 550	333±138	70±42	0.83±0.05	＜20%	PM_{10}	Cheng et al.(2008)
		α_{ap} : 630						
Xianghe, Beijing (Suburban)	03/2005	α_{sp} : 550	468±472	65±75	0.81-0.85	＜	TSP	Li et al.(2007)
		α_{ap} : 550				42.5%		
Yufa, Beijing (Suburban)	08/2006 - 09/2006	α_{sp} : 550	361±295	52±37	0.86±0.07	＜32%	PM_{10}	Garland et al.(2009)
		α_{ap} : 532						
Huairou, Beijing (Suburban)	**11/2014 - 01/2015**	**α_{sp} : 470**	**164±202**	**37±43**	**0.80±0.08**	**＜15%**	**$PM_{1.0}$**	**This work**
		α_{ap} : 470						
Shangdianzi,	09/2003 - 01/2005	α_{sp} : 525	175±189	18±13	0.88±0.05	＜60%	TSP	Yan et al.(2008)
Beijing (Rural)		α_{ap} : 525						
Pasadena, US (Rural)	05/2010 - 06/2010	α_{sp} : 532#	58±43	4±4	0.92±0.08	＜50%	$PM_{1.0}$	Thompson et al.(2012)
		α_{ap} : 532						

S6 Supporting information of the meteorological parameters and pollutant gases during the selected air pollution episode

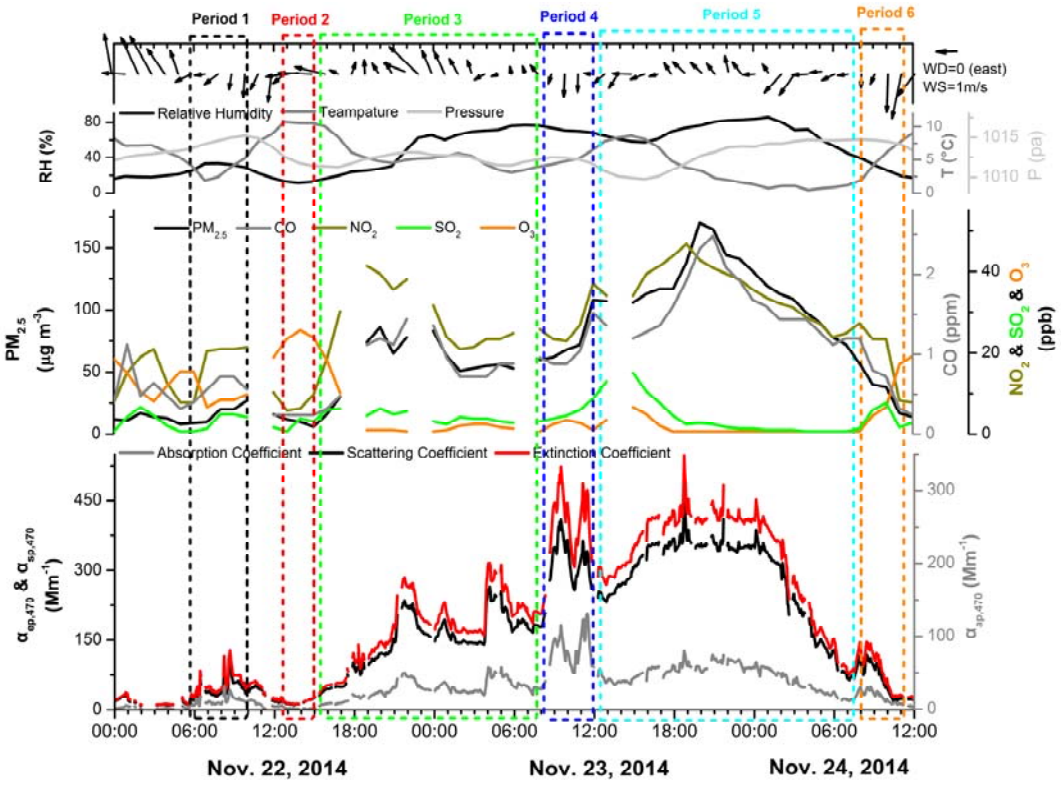

Fig. S7 Temporal wind direction and speed, temperature, relative humidity and pressure of atmosphere air, $PM_{2.5}$, CO, NO_2, SO_2 and O_3 concentrations, and the measured aerosol extinction, scattering, and absorption coefficients during the air pollution episode.

S7 EC-tracer method for the estimation of secondary organic carbon

EC is a good tracer of primary generated organic carbon (POC). Ambient OC/EC ratios larger than the OC/EC ratio of the primary ($(OC/EC)_{pri}$) indicate the formation of secondary organic carbon (SOC). The concentrations of POC and SOC can be calculated with (Turpin and Huntzicker, 1995; Lim and Turpin, 2002; Lin et al., 2009):

$$OC_{pri} = EC \times (OC/EC)_{pri} + N$$
$$OC_{sec} = OC_{tot} - OC_{pri} \quad (S9)$$

where OC_{sec} is the SOC and OC_{tot} is the measured ambient OC concentration. The concentration of POC (OC_{pri}) could be calculated by the product of measured EC concentration and the estimated $(OC/EC)_{pri}$. N is the contribution of POC from noncombustion sources or sample artifacts.

The estimation of $(OC/EC)_{pri}$ is based on the method used by Lim and Turpin (2002). The scattering plot of OC and EC concentrations for the full campaign is shown in Fig. S8. The lowest 20% percentile of ambient OC/EC ratios (shown in green dot points in Fig. S8) were used for the determination of $(OC/EC)_{pri}$. Time series of the estimated of POC and SOC mass concentrations are shown in Fig. S9.

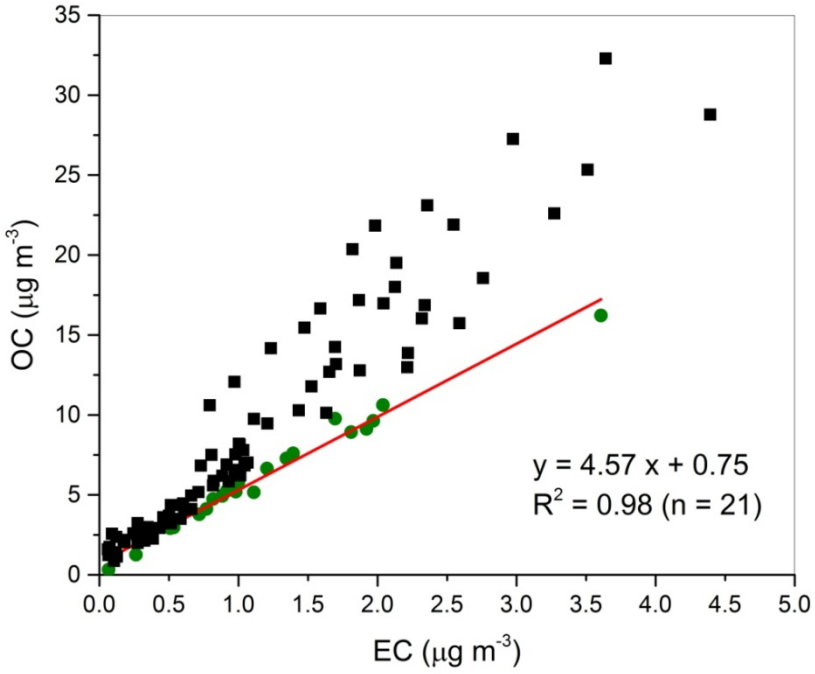

Fig. S8 Scatter plot of OC and EC concentrations. The green dot points were used to calculate the primary OC/EC.

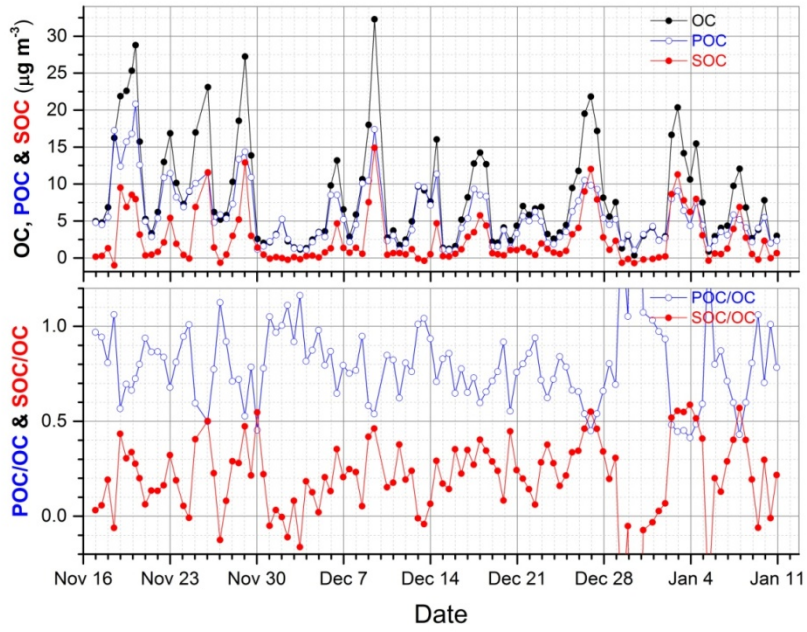

Fig. S9 Time series of (a) the measured OC mass concentrations, and the estimated primary OC (POC) and secondary OC (SOC) mass concentrations determined with EC-tracer method. (b) the percentage of POC and SOC in OC.

S8 Modification of the IMPROVE with enhanced absorption of EC

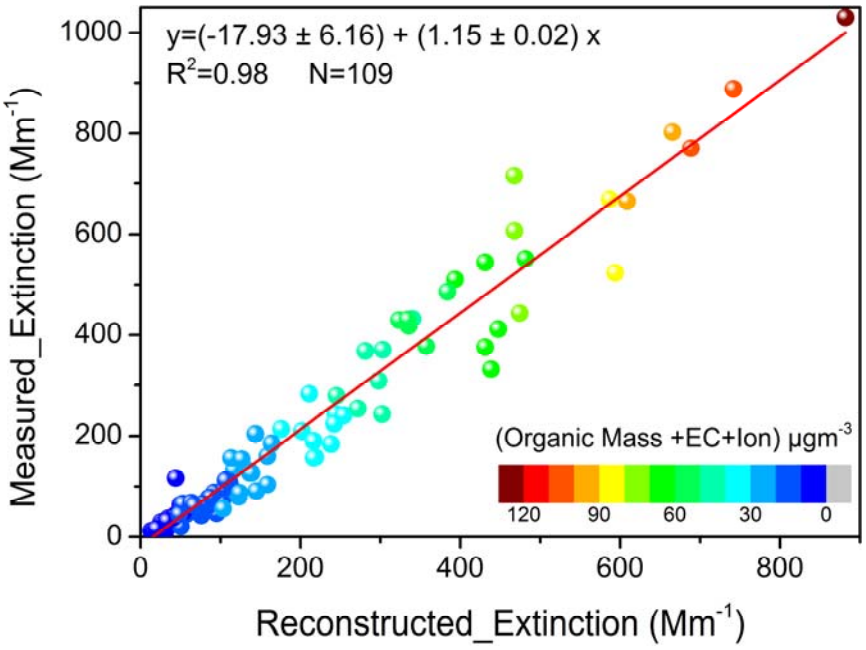

Fig. S10 Scatter plot of the measured extinction coefficient at λ = 470 nm against the reconstructed values with the new modified IMPROVE formula with MEE term of 23 m^2 g^{-1} at λ = 470 nm.

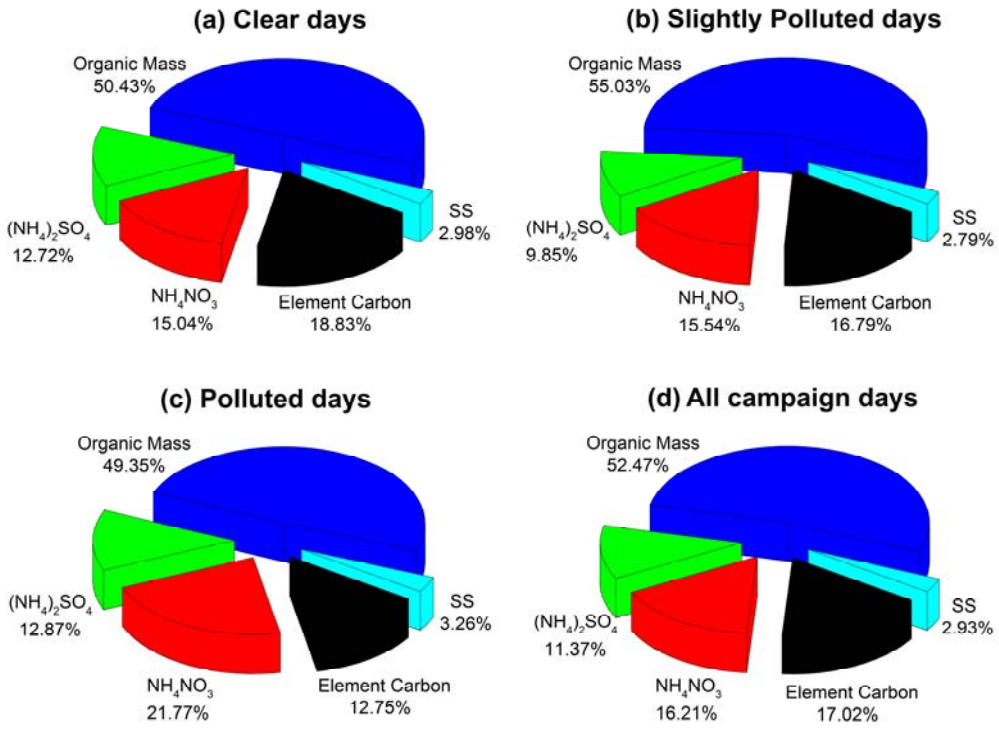

Fig. S11 Average fractional contribution of each chemical composition to dry $PM_{1.0}$ extinction coefficient with respect to different pollution level with the new modified IMPROVE formula.

References

Bohren, C. F., and Huffman, D. R. : Absorption and Scattering of Light by Small Particles; John Wiley & Sons: New York, 1998.

Cao, J. J., Wang, Q. Y., Chow, J. C., Watson, J. G., Tie, X. X., Shen, Z. X., Wang, P., and An, Z. S.: Impacts of aerosol compositions on visibility impairment in Xi'an, China, Atmos. Environ., 59, 559–566, doi:10.1016/j.atmosenv.2012.05.036, 2012.

Cheng, Y. F., Wiedensohler, A., Eichler, H., Su, H., Gnauk, T., Brüggemann, E., Herrmann, H., Heintzenberg, J., Slanina, J., Tuch, T., Hu, M., and Zhang, Y. H.: Aerosol optical properties and related chemical apportionment at Xinken in Pearl River Delta of China, Atmos. Environ., 42, 6351-6372, doi: 10.1016/j.atmosenv.2008.02.034, 2008.

Cheng, Z., Jiang, J., Chen, C., Gao, J., Wang, S., Watson, J. G., Wang, H., Deng, J., Wang, B., Zhou, M., Chow, J. C., Pitchford, M. L., and Hao, J.: Estimation of aerosol mass scattering efficiencies under high mass loading: case study for the megacity of Shanghai, China, Environ. Sci. Tech., 49, 831-838, 10.1021/es504567q, 2015.

Gao, M., Carmichael, G. R., Wang, Y., Saide, P. E., Yu, M., Xin, J., Liu, Z., and Wang, Z.: Modeling study of the 2010 regional haze event in the North China Plain, Atmos. Chem.

Phys., 16, 1673-1691, doi:10.5194/acp-16-1673-2016, 2016.
Garland, R. M., Yang, H., Schmid, O., Rose, D., Nowak, A., Achtert, P., Wiedensohler, A., Takegawa, N., Kita, K., Miyazaki, Y., Kondo, Y., Hu, M., Shao, M., Zeng, L. M., Zhang, Y. H., Andreae, M. O., and Pöschl, U.: Aerosol optical properties in a rural environment near the mega-city Guangzhou, China: implications for regional air pollution, radiative forcing and remote sensing, Atmos. Chem. Phys., 8, 5161–5186, doi:10.5194/acp-8-5161-2008, 2008.
Garland, R. M., Schmid, O., Nowak, A., Achtert, P., Wiedensohler, A., Gunthe, S. S., Takegawa, N., Kita, K., Kondo, Y., Hu, M., Shao, M., Zeng, L. M., Zhu, T., Andreae, M. O., and Pöschl, U.: Aerosol optical properties observed during Campaign of Air Quality Research in Beijing 2006 (CAREBeijing-2006): characteristic differences between the inflow and outflow of Beijing city air, J. Geophys. Res., 114, D00g04, doi:10.1029/2008jd010780, 2009.
Hand, J. L., and Malm, W. C.: Review of aerosol mass scattering efficiencies from ground-based measurements since 1990, J. Geophys. Res., 112, D16203, doi:10.1029/2007JD008484, 2007.
He, X., Li, C. C., Lau, A. K. H., Deng, Z. Z., Mao, J. T., Wang, M. H., and Liu, X. Y.: An intensive study of aerosol optical properties in Beijing urban area, Atmos. Chem. Phys., 9, 8903–8915, doi:10.5194/acp-9-8903-2009, 2009.
Li, C., Marufu, L. T., Dickerson, R. R., Li, Z., Wen, T., Wang, Y., Wang, P., Chen, H., and Stehr, J.W.: In situ measurements of trace gases and aerosol optical properties at a rural site in northern China during East Asian Study of Tropospheric Aerosols: an international regional experiment 2005, J. Geophys. Res., 112, D22S04, doi:10.1029/2006jd007592, 2007.
Li, L., Chen, J. M., Wang, L., Melluki, W., and Zhou, H. R.: Aerosol single scattering albedo affected by chemical composition: an investigation using CRDS combined with MARGA, Atmos. Res., 124, 149–157, doi:10.1016/j.atmosres.2012.11.007, 2013.
Lim, H.-J., and Turpin B. J. : Origins of primary and secondary organic aerosol in Atlanta: Results of time-resolved measurements during the Atlanta supersite experiment, Environ. Sci. Technol., 36, 4489–4496, 2002.
Lin, P., Hu, M., Deng, Z., Slanina, J., Han, S., Kondo, Y., Takegawa, N., Miyazaki, Y., Zhao, Y., and Sugimoto N. : Seasonal and diurnal variations of organic carbon in $PM_{2.5}$ in Beijing and the estimation of secondary organic carbon, J. Geophys. Res., 114, D00G11, doi:10.1029/2008JD010902, 2009.
Ma, N., Zhao, C. S., Nowak, A., Müller, T., Pfeifer, S., Cheng, Y. F., Deng, Z. Z., Liu, P. F., Xu, W. Y., Ran, L., Yan, P., Göbel, T., Hallbauer, E., Mildenberger, K., Henning, S., Yu, J., Chen, L. L., Zhou, X. J., Stratmann, F., and Wiedensohler, A.: Aerosol optical properties in the North China Plain during HaChi campaign: an in-situ optical closure study, Atmos. Chem. Phys., 11, 5959-5973, doi:10.5194/acp-11-5959-2011, 2011.
Pettersson, A., Lovejoy, E. R., Brock, C. A., Brown, S. S., and Ravishankara, A. R.: Measurement of aerosol optical extinction at with pulsed cavity ring down spectroscopy, J. Aerosol Sci., 35, 995–1011, 2004.
Pitchford, M., Malm, W., Schichtel, B., Kumar, N., Lowenthal, D., and Hand, J.: Revised algorithm for estimating light extinction from IMPROVE particle speciation data, J. Air

Waste Manage., 57, 1326–1336, doi:10.3155/1047-3289.57.11.1326, 2007.
Sun, K., Qu, Y.,Wu, Q., Han, T. T., Gu, J.W., Zhao, J. J., Sun, Y. L., Jiang, Q., Gao, Z. Q., Hu, M., Zhang, Y. H., Lu, K. D., Nordmann, S., Cheng, Y. F., Hou, L., Ge, H., Furuuchi, M., Hata, M., and Liu, X. G.: Chemical characteristics of size-resolved aerosols in winter in Beijing, J. Environ. Sci., 26, 1641–1650, 2014.
Tao, J., Zhang, L., Ho, K., Zhang, R., Lin, Z., Zhang, Z., Lin, M., Cao, J., Liu, S., and Wang, G.: Impact of PM2.5 chemical compositions on aerosol light scattering in Guangzhou-the largest megacity in South China, Atmos. Res., 135, 48–58, doi:10.1016/j.atmosres.2013.08.015, 2014.
Thompson, J. E., Hayes, P. L., Jimenez, J. L., Adachi, K., Zhang, X., Liu, J., Weber, R. J., and Buseck, P. R.: Aerosol optical properties at Pasadena, CA during CalNex 2010, Atmos. Environ., 55, 190–200, doi:10.1016/j.atmosenv.2012.03.011, 2012.
Titos, G., Foyo-Moreno, I., Lyamani, H., Querol, X., Alastuey, A., and Alados-Arboledas, L.: Optical properties and chemical composition of aerosol particles at an urban location: an estimation of the aerosol mass scattering and absorption effciencies, J. Geophys. Res., 117, D04206, doi:10.1029/2011jd016671, 2012.
Turpin, B. J., and Huntzicker, J. J.: Identification of secondary organic aerosol episodes and quantitation of primary and secondary organic aerosol concentrations during SCAQS, Atmos. Environ., 29, 3527 - 3544, 1995.
Turpin, B. J. and Lim, H. J.: Species contributions to PM2.5 mass concentrations: revisiting common assumptions for estimating organic mass, Aerosol Sci. Tech., 35, 602–610, doi:10.1080/02786820119445, 2001.
Yan, P., Tang, J., Huang, J., Mao, J. T., Zhou, X. J., Liu, Q., Wang, Z. F., and Zhou, H. G.: The measurement of aerosol optical properties at a rural site in Northern China, Atmos. Chem. Phys., 8, 2229–2242, doi:10.5194/acp-8-2229-2008, 2008.
Yang, Y. R., Liu, X. G., Qu, Y., An, J. L., Jiang, R., Zhang, Y. H., Sun, Y. L., Wu, Z. J., Zhang, F., Xu, W. Q., and Ma, Q. X.: Characteristics and formation mechanism of continuous hazes in China: a case study during the autumn of 2014 in the North China Plain, Atmos. Chem. Phys., 15, 8165-8178, doi:10.5194/acp-15-8165-2015, 2015.
Zhou, X. H., Gao, J., Wang, T., Wu, W. S., and Wang, W. X.: Measurment of black carbon aerosols near two Chinese megacities and the implications for improving emission inventories, Atmos. Environ., 43, 3918–3924, doi:10.1016/j.atmosenv.2009.03.062, 2009.